PASJ: Publ. Astron. Soc. Japan **57**, 733–741, 2005 October 25

The Schmidt Law at High Molecular Densities

Shinya KOMUGI,[1] Yoshiaki SOFUE,[1] Hiroyuki NAKANISHI,[2] Sachiko ONODERA,[1]
and
Fumi EGUSA[1]
[1]*Institute of Astronomy, The University of Tokyo, 2-21-1 Osawa, Mitaka-shi, Tokyo 181-8588*
[2]*Nobeyama Radio Observatory, Minamisaku, Nagano 384-1305*
skomugi@ioa.s.u-tokyo.ac.jp

(Received 2005 March 8; accepted 2005 August 1)

Abstract

We combined Hα and recent high-resolution ^{12}CO (J = 1–0) data to consider the quantitative relation between the gas mass and the star-formation rate, or the so-called Schmidt law in nearby spiral galaxies at regions of high molecular density. The relation between the gas quantity and the star-formation rate has not been previously studied for high-density regions, but using high-resolution CO data obtained at the Nobeyama Millimeter Array, we found that the Schmidt law is valid at densities as high as $10^3\,M_\odot\,\mathrm{pc}^{-2}$ for sample spiral galaxies, which is an order of magnitude denser than what has been known to be the maximum density at which the empirical law holds for non-starburst galaxies. Furthermore, we obtained a Schmidt law index of $N = 1.33 \pm 0.09$ and a roughly constant star-formation efficiency over the entire disk, even within several hundred parsecs of the nucleus. These results imply that the physics of star formation does not change in the central regions of spiral galaxies. Comparisons with starburst galaxies are also given. We find a possible discontinuity in the Schmidt law between normal and starburst galaxies.

Key words: galaxies: ISM — galaxies: spiral — ISM: molecules — stars: formation

1. Introduction

The global, disk-averaged star formation rate, Σ_{SFR}, and the gas density, Σ_{SMD}, in nearby galaxies are known to be well correlated, producing a simple power law called the Schmidt law: $\Sigma_{\mathrm{SFR}} \propto \Sigma_{\mathrm{SMD}}^N$ (Schmidt 1959). The determination of the index N has been extensively studied, producing values of between 1 and 2. However, the density range at which this law holds for normal galaxies has not been studied as much. The lower density cutoff for the Schmidt law has been argued by Kennicutt (1989) based on gravitational instability, giving a critical gas density of 5 to $10\,M_\odot\,\mathrm{pc}^{-2}$, where star formation is strongly suppressed below this limit. On the other hand, there has been only marginal success for the observational consideration of the Schmidt law at higher densities. This is primarily due to the limit in spatial resolution of CO observations, where the ^{12}CO (J = 1–0) emission at $\lambda = 2.6$ mm is used as a tracer of molecular gas.

High molecular density regions are spatially small in general, owing to the molecular cloud's patchy structure and central condensation (Sakamoto et al. 1999). Therefore, it is essential to make CO observations with smaller beam sizes (higher resolution). Rownd and Young (1999) have shown that the Schmidt law holds better when sampled within galaxies, using 45″ resolution data at the center of over 100 nearby galaxies (see figure 11 in Rownd, Young 1999). However, the densest gas in galaxies is normally confined to within a few hundred parsecs of the nucleus (e.g., Sakamoto et al. 1999; Sofue et al. 2003a). Therefore, a 45″ resolution, which corresponds to kpc scales in nearby galaxies, is too large to consider the validity of the Schmidt law at the highest densities. Kennicutt (1998) has shown that the Schmidt law holds at higher densities if we include a sample of IR luminous starburst galaxies with $L_{\mathrm{FIR}} \sim 10^8$–$10^{10}\,L_\odot$ to $L_{\mathrm{FIR}} \leq 10^{12}\,L_\odot$ at high molecular densities. Including this sample has extended the Schmidt law up to an unchallenged value of $\Sigma_{\mathrm{SMD}} \sim 10^5\,M_\odot\,\mathrm{pc}^{-2}$ (see figure 6 in Kennicutt 1998). However, IR luminous starbursts represent special physical conditions that display a systematic difference from normal spirals, and including this sample in considering the validity of Schmidt law may lead to a misunderstanding of the physical properties that underlies the poorly understood power law. Gao and Solomon (2004) have indeed found that the IR luminous galaxies with $L_{\mathrm{IR}} \leq 10^{11}\,L_\odot$ display a systematic difference from normal galaxies in view of Schmidt law, in that the ratio of HCN to CO rises abruptly for IR luminous galaxies compared to normal galaxies. Excluding these IR luminous samples from Kennicutt (1998) and considering only normal spirals reveal that the law is only valid up to $\sim 10^2\,M_\odot\,\mathrm{pc}^{-2}$. Other studies of the Schmidt law at high densities involve HCN (Gao, Solomon 2004) and higher transition emission, such as ^{12}CO (J = 2–1), as probes of hydrogen at higher densities. However, the weakness of this emission and the difficulty in comparing Σ_{SMD} derived from these probes and others of lower density [such as CO (J = 1–0) and H I] has limited any consistent consideration of Schmidt law's validity at a wide density range.

In order to approach a more fundamental understanding of the relation between the gas content and star formation, it is essential to know to what density the Schmidt law holds for normal galaxies, or whether the simple power-law formulation of the Schmidt law is valid at all. This will require that we use

Table 1. Basic properties of the sample galaxies.*

Galaxy	RA	Decl	Type	D (Mpc)	i (°)	Size ($'$)
(1)	(2)	(3)	(4)	(5)	(6)	(7)
NGC 2903	09 29 19.9	+21 43 19	SAB	6.3	60	11.2
NGC 3593	11 11 59.2	+13 05 28	SA	5.5	67	4.9
NGC 4041	11 59 38.7	+62 25 03	SA	22.7	18	2.9
NGC 4192	12 11 15.4	+15 10 23	SAB	16.8	74	7.8
NGC 4212	12 13 06.4	+14 10 45	SA	16.8	47	2.9
NGC 4254	12 16 16.9	+14 41 46	SA	16.8	28	5.5
NGC 4303	12 19 21.4	+04 44 58	SAB	16.8	25	6.2
NGC 4321	12 20 23.2	+16 06 00	SAB	16.8	28	7.1
NGC 4419	12 24 25.1	+15 19 28	SB	16.8	67	2.8
NGC 4501	12 29 28.1	+14 41 50	SA	16.8	58	6.3
NGC 4535	12 31 47.9	+08 28 25	SAB	16.8	43	6.6
NGC 4536	12 31 53.5	+02 27 50	SAB	16.8	67	6.5
NGC 4548	12 32 55.1	+14 46 20	SB	16.8	37	5.4
NGC 4569	12 34 18.7	+13 26 18	SAB	16.8	63	8.3
NGC 4579	12 35 12.6	+12 05 40	SAB	16.8	37	5.4
NGC 4654	12 41 25.7	+13 23 58	SAB	16.8	52	4.4
NGC 4689	12 45 15.3	+14 02 13	SA	16.8	30	4.1
NGC 4736	12 48 32.4	+41 23 28	SA	4.3	35	11
NGC 4826	12 54 16.9	+21 57 18	SA	4.1	57	9.3
NGC 5005	13 08 37.6	+37 19 25	SAB	21.3	62	4.8
NGC 5194	13 27 46.9	+47 27 16	SA pec	7.7	20	10.5
NGC 5248	13 35 02.4	+09 08 23	SAB	22.7	42	6.3
NGC 6946	20 33 48.8	+59 58 50	SAB	5.5	30	13.2

* Units of right ascension are hours, minutes, and seconds, and units of declination are degrees, arcminutes, and arcseconds. Col.(1): Galaxy name. Col.(2), (3): Galaxy coordinates (epoch 1950). Col.(4): Hubble type, taken from RC2. Col.(5): Distance to the galaxy, adopted from Ho et al. (1997). Col.(6): Inclination angle, given in Young et al. (1995). Col.(7): Projected diameter, taken from Rownd and Young (1999).

a consistent probe of the gas, at a wide density range.

In this study, we consider the validity of the Schmidt law, including densities above this limit by using recent high-resolution single-dish and interferometry observations. Section 2 provides information on CO and Hα data, and the procedures for calculating $\Sigma_{\rm SMD}$ and $\Sigma_{\rm SFR}$. In section 3 we show the result, and in section 4 we discuss the various uncertainties that are related to the Schmidt law, and the validity of the Schmidt law at high densities. Conclusions are given in section 5.

2. Data

We made high-resolution (typically $3''$) ^{12}CO (J = 1–0) observations of galaxies in the Virgo Cluster, with the NMA (Nobeyama Millimeter Array). The observational parameters and data are presented in Sofue et al. (2003a). Using the obtained data and other high-resolution CO data obtained mainly at NRO (Nobeyama Radio Observatory), and further combining it with low-resolution single-dish observations in other studies to account for intermediate gas density regions, we studied the validity of the Schmidt law over a wide density range within 23 spiral galaxies. Fundamental parameters of the sample galaxies are listed in table 1.

2.1. Sample Selection

Rownd and Young (1999) found that the Schmidt law holds better when data are sampled locally within galaxies, with a smaller beam size. However, their study used CO and Hα data at $45''$ resolution, too large to consider high-density regions, which are typically small in size. In order to consider the Schmidt law for a wide range of gas density, we chose galaxies that have been observed in several beam sizes. Twenty three spiral galaxies were chosen, 14 of which are members of the Virgo Cluster. All are spirals, SA, SAB, or SB in morphology. Most samples have 3 data points corresponding to different beam sizes, expressing different density ranges. Some galaxies have been observed in more beam sizes. NGC 4254, NGC 4321, NGC 4501, NGC 4548, and NGC 4579 have 4 data points, and NGC 4303, NGC 4535, and NGC 4569 have 5 data points. The inclination angle, $i(^\circ)$, total blue magnitude, $B_{\rm tot}$, and peak ^{12}CO (J = 1–0) line antenna temperature, $T_{\rm A}^*$ (mK) are in the range $18 \leq i \leq 74$, $8.99 \leq B_{\rm tot} \leq 12.08$, and $21 \leq T_{\rm A}^* \leq 312$, respectively.

2.2. CO Data

The CO and Hα data used in this study are listed in table 2. Much of the interferometric data were obtained during the course of the "Virgo High-resolution CO Survey", a long-term project at Nobeyama Millimeter Array (Sofue et al. 2003a).

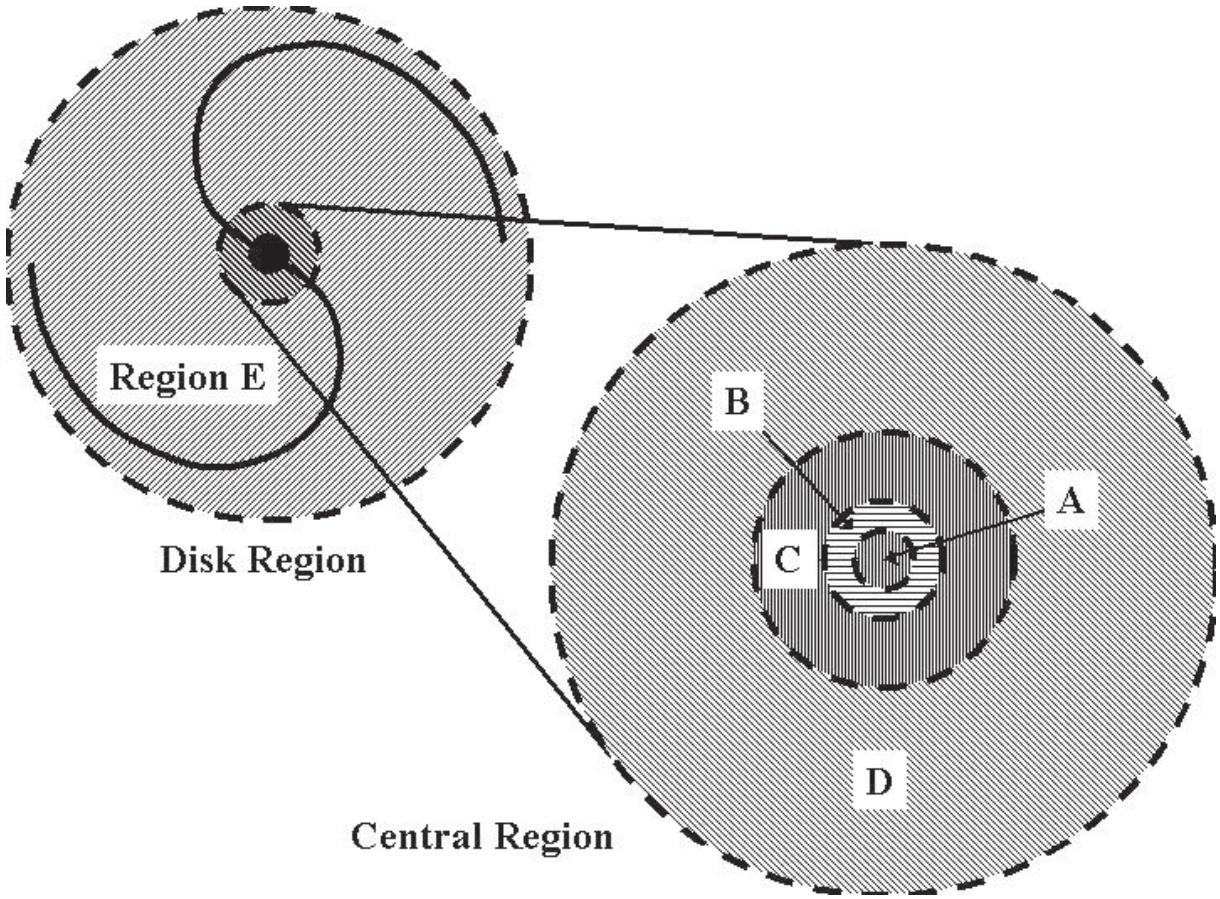

Fig. 1. Schematic picture of regions A through E. The dotted lines indicate the edge of each of the regions. The regions are scaled using an arbitrary global diameter (edge of region E) of 5″ (the average for Virgo galaxies).

We combined data with different spatial resolutions, so that data with low resolution, which averages a large area within the galaxy, would give low density values, whereas high-resolution data at galactic centers would give high molecular densities. Molecular gas densities in the literature were recalculated using a conversion factor of $X_{\rm CO} = 2.0 \times 10^{20}$ ($\rm cm^{-2}\,K^{-1}\,km^{-1}\,s$) and the formulation

$$\left[\frac{\Sigma_{\rm SMD}}{\rm g\,cm^{-2}}\right] = 2 \times \left[\frac{m_{\rm H}}{\rm g}\right] \times X_{\rm CO} \left[\frac{I_{\rm CO}}{\rm K\,km\,s^{-1}}\right] \times 1.6, \qquad (1)$$

where $m_{\rm H}$ and $I_{\rm CO}$ are the mass of a hydrogen atom and the CO intensity, respectively. $X_{\rm CO}$ is poorly understood for the sample galaxies, and the value we adopt is the mean value of those derived for our galaxy and other disk galaxies (e.g., Sanders et al. 1984; Bloemen et al. 1986; Solomon et al. 1987; Nakai, Kuno 1995). The factor 1.6 accounts for the mass of heavy elements. The gas densities for each of the regions within the galaxies were derived in the following manner:

1. The highest resolution data ($\sim 3''$, see table 2) was used to derive the gas mass at the central-most region. We call this region A.
2. Then, the second-highest resolution data (6″, 16″, or 45″, the highest for the individual galaxy for which we retrieved data), which was also centered on the nucleus, was used to derive the gas mass within the beam.
3. The gas mass derived from 1 was subtracted from that derived in 2. This would give the gas mass confined within the annulus corresponding to the difference in the area of the two beam sizes. We call this region in the annulus B.
4. The same procedures, 1 through 3, were repeated for larger beam sizes, and then the surface gas densities were derived for each of the annuli. Each of the annuli are labeled C, D, and E, respectively, in order of increasing beam size. Note that region E uses the global averaged value, and is not actually derived from a single beam.

This procedure divides the galaxy into several annuli, so that the derived gas densities give radial-dependent values. We present a schematic picture of the regions in figure 1.

2.3. *Hα Data*

The calculation of the star-formation rate $\Sigma_{\rm SFR}\,M_\odot\,\rm pc^{-2}\,yr^{-1}$ was conducted following Kennicutt (1998), using the Hα luminosity emitted from ionized gas around young massive stars:

$$\left[\frac{\Sigma_{\rm SFR}}{M_\odot\,\rm pc^{-2}\,yr^{-1}}\right] = \left[\frac{L({\rm H}\alpha)}{1.26 \times 10^{41}\,\rm erg\,s^{-1}}\right] \times \left[\frac{S}{\rm pc^2}\right]^{-1}, \qquad (2)$$

where S is the projected area of Hα emission. Procedures the

Table 2. CO and Hα references.*

	Region	CO	Hα
Global average	E	(1)	(1)
central 45″	D	(2)	(2)
central 16″	C	(3)	(4)
central 6″	B	(5)	(4)
central 3″	A	(6), (7)	(8)

* References (1) Young et al. (1996), (2) Rownd and Young (1999), (3) Nishiyama and Nakai (2001), (4) Koopmann et al. (2001), (5) Helfer et al. (2003), (6) Sakamoto et al. (1999), (7) Sofue et al. (2003a), (8) Ho et al. (1997). Data for the central 6″ were retrieved only for NGC 4303, NGC 4321, NGC 4535, NGC 4548, and NGC 4569. Data for the central 16″ were retrieved only for NGC 4254, NGC 4303, NGC 4501, NGC 4535, and NGC 4569. Global average, central 45″ and 3″ data were retrieved for all of the sample galaxies. Data from (2), (4), (6), and (7) were traced from radial profiles given in the reference. For galaxies that overlapped in (6) and (7), data from Sofue et al. (2003a) were used.

same as that for the CO data (1 thorough 4) were applied to the Hα data for the calculation of $\Sigma_{\rm SFR}$.

Galactic extinction was corrected for all of the data. Since the original references in table 2 adopt different extinction laws, data from theses references were recalculated using the same form of $A(\mathrm{H}\alpha) = 0.08\,(\csc|b| - 1)$ in magnitudes, were b is the galactic latitude (regions A, D, and E). In the original references, galactic extinction for regions B and C were corrected using Landolt standards (Landolt 1992) or the standard extinction curve at Kitt Peak National Observatory or Cerro Tololo Inter-American Observatory. Because the references for regions B and C do not list the standard stars or the data before correction, the corrected data from the original references were used without adopting the same extinction law. This did not cause any significant changes; because the typical extinction due to the Galaxy is of order 0.01 to 0.1 mag, this will be only 0.004 to 0.04 on the ordinate (see the following figures). We therefore conclude, that the galactic extinction for the samples was satisfactorily corrected.

The reader should refer to the original references (see table 2) for details. Extinction within the sample galaxies (internal extinction) plays a role in the determination of the true Hα luminosity at the central regions of galaxies. The effects of internal extinction correction will be discussed in section 4.

3. Results

Figure 2 shows the $\Sigma_{\rm SMD}$ versus $\Sigma_{\rm SFR}$ on a logarithmic scale, for each of the regions in the sample galaxies. We clearly see that the data plotted with smaller beam sizes account for the high-density regime of the Schmidt law, extending to densities as high as $10^3\,M_\odot\,\mathrm{pc}^{-2}$. For the highest densities, the data seem to be dispersed from the correlation. However, we find that galaxies that are dispersed from the correlation are those in the sample whose distances are closer to our Galaxy; namely, NGC 3593, NGC 4736, NGC 4826, NGC 6946 are only several Mpc away compared to 16.8 Mpc for most of the sample. The resolution of 3″ corresponds to under 100 pc for these galaxies. An investigation of the coordinates of the center of these galaxies in Hα and CO will reveal that the CO intensity peaks are offset from the Hα centers, often by more than 3″. We excluded these galaxies in further analysis because there was a possibility that a small beam of ∼ 3″ does not include both the star-forming region and its counterpart molecular cloud, which is generally several×10 pc in size. In general, star-forming regions do not coincide with the molecular clouds that give birth to them. This is seen in spiral arms, where the optical and molecular spiral structures are offset. If only the molecular clouds are observed, and not the star-forming regions, which are physically coupled to it, it would result in the gas density to show excess from the expected correlation. The data points for the 4 galaxies named above, seem to have this property. Although not significantly different from the other galaxies, NGC 2903 and NGC 5194, which have similar spatial resolutions (under 100 pc) in region A were also excluded. Moreover, it should be noted that the Hα luminosities of NGC 4736, NGC 4826, NGC 5194, and NGC 6946 were only given as lower limits in Ho et al. (1997). This leaves a subset of 17 galaxies in our sample. The same figure, but with these galaxies excluded, is shown in figure 3. A tighter correlation can be seen through the gas density range. Figure 3 clearly shows that high density regions A, B, and C, and the lower density regions D and E, can be fitted with the same line. A least-squares fit to figure 3 yields a Schmidt law index, N, of 1.14 ± 0.08, allowing for errors in both of the axes.

4. Discussion

4.1. Error Estimation

(1) Derivation of $\Sigma_{\rm SMD}$

In general, we refer to gas mass as the total of both the molecular and atomic masses. However, the legitimacy of using either or both of the hydrogen gas is not well known. While Kennicutt (1989) found that the total gas density correlates better with the star-formation rate, others, such as Gao and Solomon (2004), believe that denser (hence, H_2 rather than H I) gas correlates better. Boissier et al. (2003) find that the total and the molecular gas both correlate well with $\Sigma_{\rm SFR}$, but the tight correlation seen in using the total gas is driven by the correlation of the molecular gas with the star-formation rate. The recent trend seems to be in favor of using only molecular gas, but it is still controversial. We used only molecular gas in our study, on the following grounds: (1) massive star formation presumably occurs in molecular clouds cores, where H I is less abundant. From the standpoint that star formation is a two-step process, where H_2 clouds are first formed from H I, and stars are then formed from H_2, we conclude that H_2 should be a more direct tracer of the star-formation rate. (2) We are interested in high-density regions of galaxies, and have used galactic centers. Because these regions are known to be H I deficient, even if H I plays a role in star formation, its mass should be negligible.

Another uncertainty resides in the CO-to-H_2 conversion factor, $X_{\rm CO}$. The constant value of $X_{\rm CO} = 2.0 \times 10^{20}$ is highly questionable. However, the conversion factor for each of the sample galaxies is not known, and moreover it's variation within those galaxies are potentially difficult to know; we have used the average value of our Galaxy and galaxies with known

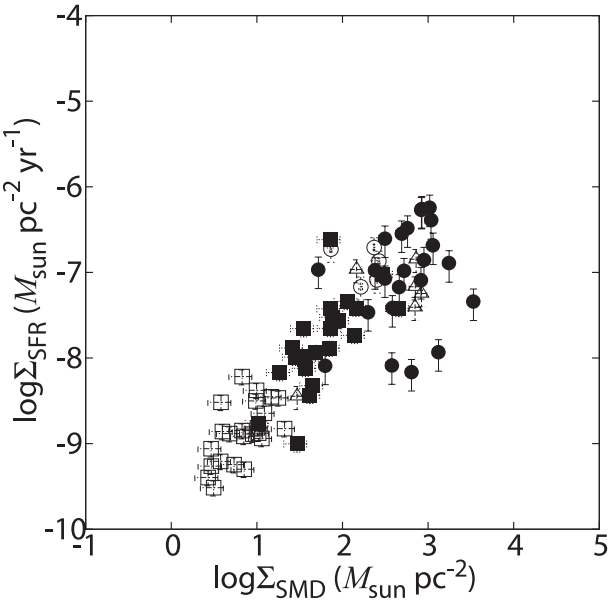

Fig. 2. Σ_{SMD}–Σ_{SFR} for all of the sample galaxies. Internal Hα extinction has not been corrected. The abscissa is $\log \Sigma_{SMD}$, and the ordinate is $\log \Sigma_{SFR}$. The filled circles, triangles, open circles, filled squares, and open squares stand for regions A, B, C, D, and E, respectively. The horizontal error bars for filled circles lie within the symbol. Notice that several points in region A are deviated from other plots.

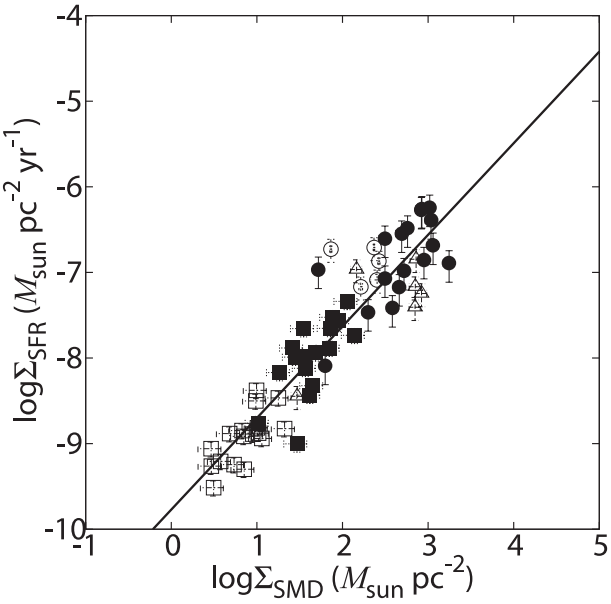

Fig. 3. Same as figure 2, with NGC 2903, NGC 3593, NGC 4736, NGC 4826, NGC 5194, and NGC 6946 excluded, as mentioned in section 3. A best fit yields $N = 1.07 \pm 0.06$.

X_{CO} uniformly for all of the data for the sake of simplicity. Boissier et al. (2003) found that by using metallicity dependent X_{CO}, Σ_{SMD} should typically change by a factor of 2 to 3 in the central regions compared to disk regions of nearby spirals, in the sense of decreasing gas mass. This, however, does not cause any disastrous changes compared to using a constant conversion factor, because factors of 2 to 3 makes little difference to the positions in which data are plotted on the $\log \Sigma_{SMD}$–$\log \Sigma_{SFR}$ scale. Again, we adopted the constant X_{CO} for the sake of uniformity and simplicity.

The highest resolution measurements use interferometers, which have the "missing flux" problem. Spatially extended sources can not be detected, which has the effect of underestimating the surface density. Figure 3 indicates that compared to region D with 45″ resolution, regions A and B with the interferometric observations are typically an order of magnitude higher in Σ_{SMD}. Even compared to region C with 16″ resolution, region A is higher, typically by a factor of about 3. This indicates that the missing flux has no significant effect on Σ_{SMD}.

The horizontal error bars in figure 3 do not include the uncertainties given above. They are typically 15% to 30%, and are mainly due to errors in the flux calibration, given in the original references.

(2) Hα extinction

The Hα emission lines are subject to extinction within the target galaxies, and we must also account for this in the analysis. A global, uniform extinction correction of ~ 1 mag is suggested by Kennicutt and Kent (1983), but this is an oversimplification, because central regions of galaxies are generally thought to be subject to larger extinction than disk regions. The extinction for region A can be calculated from $E(B-V)$ magnitudes given in Ho et al. (1997), but extinction for the other regions, B through E, are not known.

An extinction model where the extinction increases in proportion to the hydrogen column number density, N_H may be used for these regions. Using $N_H = 2 \times 10^{21} A_V$ (Schultz, Wiemer 1975; Bohlin et al. 1978; Sneden et al. 1978; Kent et al. 1991), and $N_H = X_{CO} I_{CO}$, the Hα extinction, A_R, can be calculated by $A_R = 0.75 A_V$ (Rieke, Lebofsky 1985). We assume that N_H is dominated by molecular hydrogen, because H I and H_2 are generally spatially offset in galaxies disks, divided by a transition region. As long as we calculate Σ_{SMD} using only H_2, H I should only play a minor role in the extinction, even when calculating global values in region E. However, this extinction model is known to yield overestimates in regions of higher density (Wong, Blitz 2002), and will give unrealistic values of the A_R magnitude up to 5 mag in region C, 10 mag in region B, and even more in region A. This is clearly an overestimation, because the gas consumption timescale, τ, derived for these regions using this correction (see subsection 4.4) will yield τ of only several hundred years, too short to explain the many number of galaxies with such star-forming central regions. Therefore, we adopted the same extinction as that derived in region A, for regions B and C. For regions D and E, the extinction model explained above was adopted. A source of uncertainty in applying extinction based on molecular density for regions D and E, are the difference in the resolution for CO and Hα measurements. Light from H II regions is absorbed by dust associated with molecules that are directly between the observer and the H II region in the line of sight. However, the observing beam of the CO observation is far larger than that of the Hα observation. Therefore, we can only apply an extinction correction based on the average gas density of the

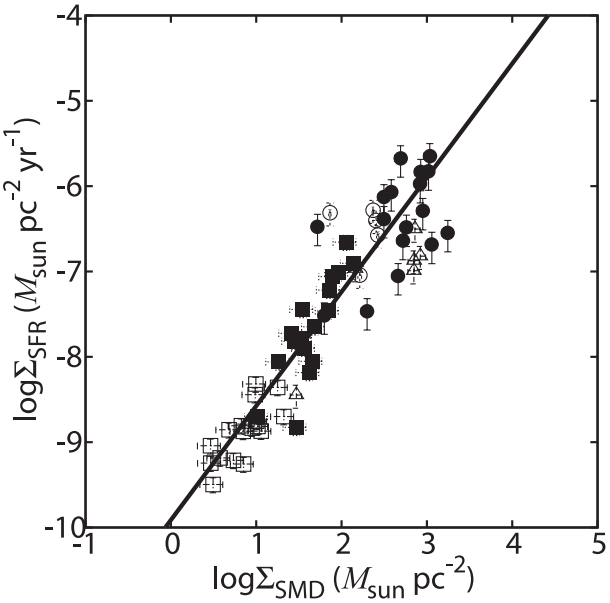

Fig. 4. Same figure as 3, but corrected for Hα extinction. A best fit yields $N = 1.33 \pm 0.08$.

region within this CO beam size, whereas the actual extinction of Hα light occurs on a smaller scale. This may cause the extinction correction to be an underestimate, but a true correction is impossible unless the Hα emitting region is completely resolved in the CO observation. In the case of regions D and E, where the beam size is 45″, this effect may not be negligible. However, because existing CO observations cannot resolve individual H II regions, we do not further refer to this problem. The effect of neglecting this possible underestimation is discussed briefly in subsection 4.2.

Figure 4 is the same as figure 3, with the extinction corrected as explained above. A least-squares fit yields $N = 1.33 \pm 0.09$, higher than $N = 1.14 \pm 0.08$ for no extinction correction. Even with the extinction corrected, however, N is lower than the widely accepted value of 1.4 given by Kennicutt (1998), which includes IR luminous starbursts at dense gas regimes.

Other errors are as follows: Hα data used in region D was traced from figure 2 in Rownd and Young (1999), and regions B and C from figure 5 in Koopmann et al. (2001). We assigned an error of 0.1 on the ordinate of these data. Other errors are mainly due to difficulty in continuum subtraction. See original paper for details.

4.2. Σ_{SMD}–Σ_{SFR} Relation

A least-squares fit to figure 4 resulted in

$$\log \Sigma_{\rm SFR} = (1.33 \pm 0.09) \log \Sigma_{\rm SMD} - 9.95 \pm 0.2, \quad (3)$$

and a best fit to the same data using only region E, or the disk, resulted in

$$\log \Sigma_{\rm SFR} = (1.51 \pm 0.6) \log \Sigma_{\rm SMD} - 10.19 \pm 0.4. \quad (4)$$

Similarly, a best fit using only regions A, B, C, and D, or the central regions, yields

$$\log \Sigma_{\rm SFR} = (1.22 \pm 0.15) \log \Sigma_{\rm SMD} - 9.68 \pm 0.4 \quad (5)$$

The index and the constant of the fits for the disk and central regions are both well within the range of error, although the errors for each of the regions are large. This is consistent with the idea that the data plots in the central regions have the same Schmidt law as in the disk regions.

The beam size of the highest density region A (typically 3″) corresponds to a projected scale of 250 pc for galaxies in the Virgo cluster. The Schmidt law is thought to be an empirical law that holds at kpc scales within galaxies, but our results imply that smaller scales of several hundred parsecs may still be valid when considering the Schmidt law. It may be noted that regions close to the nucleus are subject to physical conditions different from the disk. Besides the dense gas tracers, such as HCN and CO (J = 2–1), observed in these regions, rotation curves in the central kpc are also known to be different from disks, in that the rotation becomes nearly rigid compared to nearly flat in the disks (Sofue et al. 2003b). This would lessen the effect of shear, which works on the clouds, and may change the efficiency of star formation based on gravitational collapse. These effects could work to cause a systematic change in the relation between the gas content and the star-formation rate in the central regions. However, the index N of the Schmidt law that we derived from the least-squares fitting in figure 4 indicates no systematic difference in the Schmidt law within the range of error. We conclude that the validity of the Schmidt law at densities from $10^0\,M_\odot\,{\rm pc}^{-2}$ up to $10^3\,M_\odot\,{\rm pc}^{-2}$ does not change.

It is difficult to consider the Schmidt law for normal galaxies at even higher densities, because doing this would require that we observe with even better spatial resolution, which in turn, would give rise to the problem that we may not be able to observe the molecular cloud and its counterpart star forming region within one beam, as we have seen in section 3 with galaxies at several Mpc from us. As can be understood from this example, the Schmidt law is fundamentally a correlation seen when averaged over a considerable scale. It may be said that this linear correlation breaks down when averaged over an area of under $\sim 10^2$ pc. Thus, for higher densities, we must use IR luminous galaxies that have unusually high molecular densities, like in the studies by Kennicutt (1998). A superposition with these IR luminous starbursts from Kennicutt (1998) and our study is shown in figure 5. Error bars are not shown, but are the same as in figure 4. The high-density end of normal galaxies exhibits similar $\Sigma_{\rm SMD}$ and $\Sigma_{\rm SFR}$ as the lower density end of the starbursts, but the starbursts display higher $\Sigma_{\rm SFR}$ compared to the Schmidt law derived for normal galaxies at densities above $\Sigma_{\rm SMD} = 10^3\,M_\odot\,{\rm pc}^{-2}$. It is important to bear in mind, though, that $\Sigma_{\rm SFR}$ of the IR starbursts have been derived from IR luminosities, possibly introducing inconsistencies between the Hα-derived rates. $\Sigma_{\rm SFR}$ derived from Hα will indeed give a lower $\Sigma_{\rm SFR}$ if extinction is not corrected. However, we corrected for Hα extinction in our analysis, and Kewley et al. (2002) found that the star-formation rates derived from extinction corrected Hα and FIR luminosities agree well. Therefore, this systematic difference between starbursts and normal galaxies that we see in figure 5 may indeed be real, implying that, again, we must establish a relation between the gas and the star-formation rates for normal galaxies first in order to gain fundamental knowledge of the

Table 3. The Schmidt law index.*

Region	Hα extinction correction	N	$\log A$
All	No	1.14 ± 0.08	-9.87 ± 0.20
All	Yes	1.33 ± 0.09	-9.95 ± 0.20
E	Yes	1.51 ± 0.60	-10.19 ± 0.4
A+B+C+D	Yes	1.22 ± 0.15	-9.68 ± 0.4
Kennicutt (1998)	Yes	1.31 ± 0.04 (1.4 ± 0.15)	-9.45 ± 0.07 (-9.61 ± 0.13)
Starbursts	No (IR)	1.28 ± 0.08	-9.09 ± 0.24

* Schmidt law index and the constant for various regions in our study, and that derived by Kennicutt (1998). A constant value of 1.1 mag was adopted for Hα extinction in Kennicutt (1998). The values for Kennicutt (1998) were changed to include only molecular gas, whereas the values in parentheses are from the original paper.

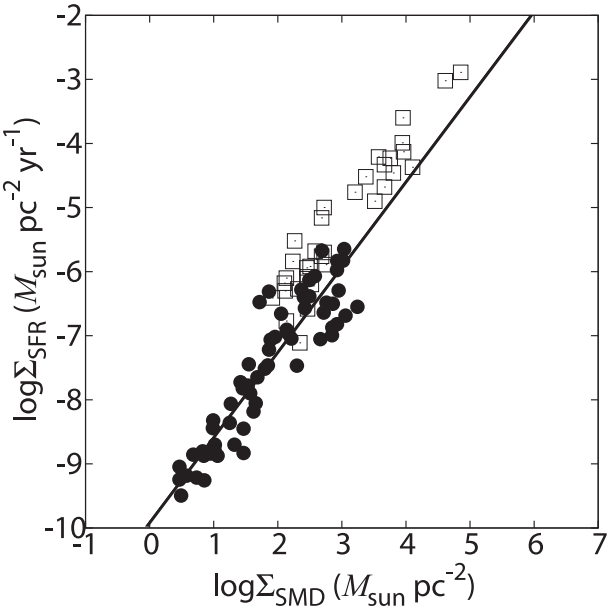

Fig. 5. Composite Schmidt law. The filled circles are the normal galaxies in this study, and the open squares are the IR luminous starbursts from Kennicutt (1998). The line is a best fit only to normal galaxies. Notice that the starbursts are systematically offset from the Schmidt law of normal galaxies in the sense of a higher Σ_{SFR}. A best fit for both of the data together will yield $\log \Sigma_{SFR} = (1.41 \pm 0.07) \log \Sigma_{SMD} - 9.83 \pm 0.18$.

relation between the gas content and the star-formation rate. A least-squares fit to the normal and starbursts together, gives $N = 1.41 \pm 0.07$, consistent with the "composite" Schmidt law derived by Kennicutt (1998).

It is justified to say that the derived slope of $N = 1.33$ is relatively reliable, despite the unquantifiable uncertainties, such as X_{CO}, the missing-flux problem stated in subsection 4.1, and the problem of underestimating Hα extinction, stated in subsection 4.2. This is because allowing for a systematic increase in X_{CO} by a factor of 3 with galactocentric radius will raise the slope while, on the other hand, correcting for the missing flux and underestimated extinction would increase the density slightly in regions A and B and the star-formation rate in regions D and E, resulting in the decrease of the slope. These effects would offset each other to some extent, and changes in the slope would not be very significant. The comparison with starbursts and normal galaxies would not be significantly affected, because the results by Kennicutt (1998) would also have to be corrected in accordance.

4.3. Interpretation of the Schmidt Law Index N

The widely accepted value of $N = 1.4$ by (Kennicutt 1998) is unchallenged regarding its density range of order ~ 5, and a simple interpretation of this index is often given that the star-formation rate volume density, ρ_{SF}, scales with gas volume density, ρ_{gas}, divided by the free-fall timescale of the gas cloud, $t_{ff} \propto \left(\sqrt{G\rho_{gas}}\right)^{-1}$. This gives

$$\rho_{SF} \propto \frac{\rho_{gas}}{\left(\sqrt{G\rho_{gas}}\right)^{-1}} \propto \rho_{gas}^{1.5}, \tag{6}$$

which may explain the value of $N = 1.4$. However, this explanation assumes that we are observing a single gas cloud as it gravitationally collapses, and eventually forms a star. In actual observations, we are observing an area of the galaxy with a beam having scales of several hundred parsecs. Naturally, it is not possible to observe a single cloud, but instead the observer is averaging the gas density and the star-formation rate of many clouds, which are typically several $\times 10$ parsecs in linear scale. On such scales, the increase in the gas density, ρ_{gas} (or, Σ_{SMD}), should not be interpreted as an increase in the density of the individual clouds. Instead, we should regard the change as being an increase in the number of molecular clouds within that beam. Therefore, as long as the observing beam is much larger than the typical size of a single molecular cloud, Σ_{SFR} should increase in proportion to Σ_{SMD}, giving $N = 1$ as the natural result. A best fit to the IR starbursts from Kennicutt (1998) will give $N = 1.28 \pm 0.08$, similar to that for the normal galaxies in our study. However, the factor A of the Schmidt law (provided $\Sigma_{SFR} = A\Sigma_{SMD}^{N}$), determined by the y-axis intercept of figure 5, is higher for these starbursts compared to the normal galaxies, as can be clearly seen from figure 5 with $\log A = -9.09 \pm 0.24$. The datasets for the starbursts were recalculated using the same X_{CO} as in this study. The transition in the Schmidt law from normal galaxies to starbursts seems to be step-like, or that there are two systems in the Schmidt law, with systematically different star-formation rates.

4.4. The Star Formation Efficiency

It is convenient to define the star-formation efficiency (SFE) by

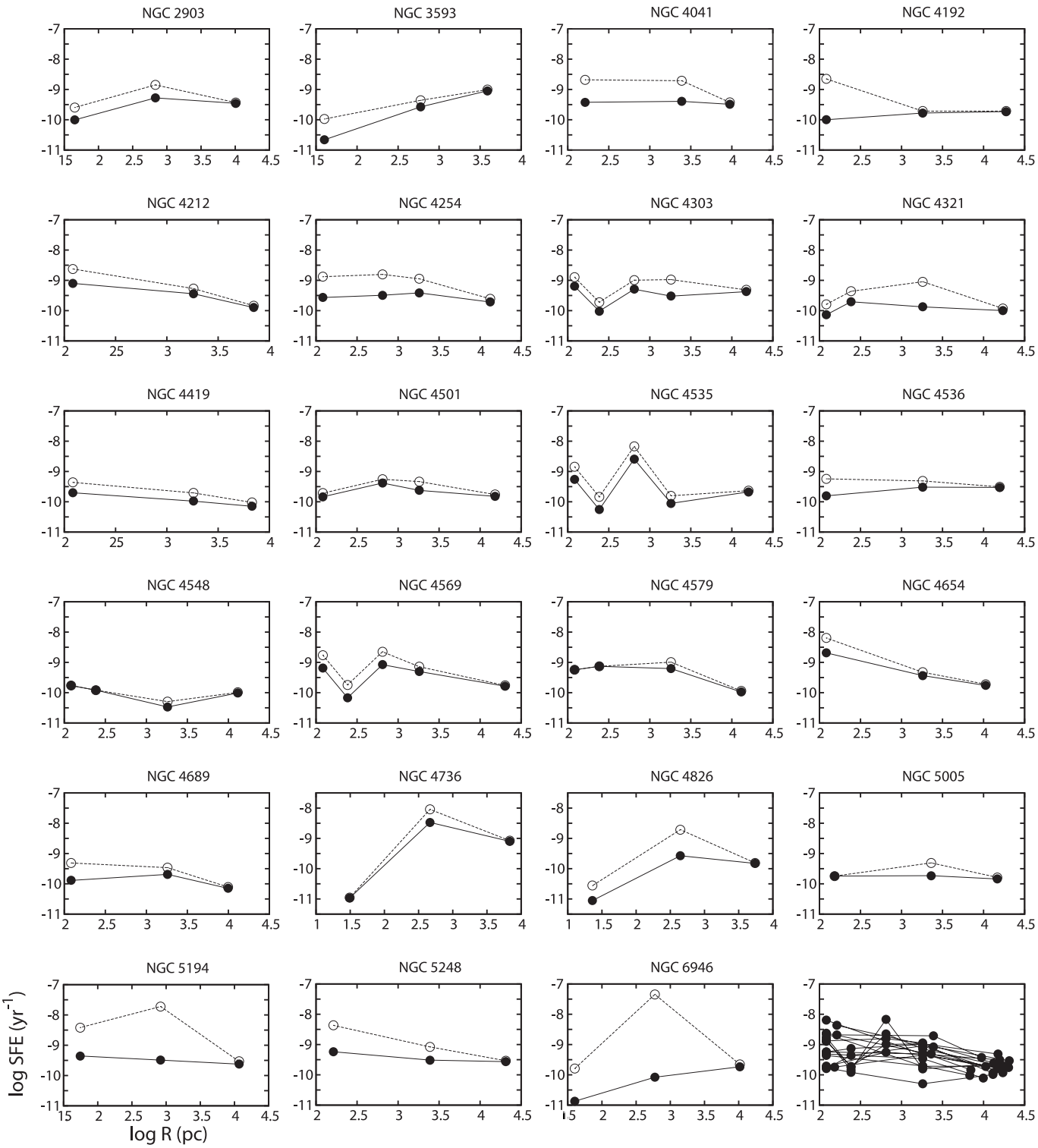

Fig. 6. Star-formation efficiency (SFE), galactocentric radius, for all of the sample galaxies. The filled circles are data with no Hα extinction correction, and the open circles are extinction-corrected data following the method shown in section 4. The bottom-right figure is a superposition of the subset of 17 sample galaxies, all corrected for extinction.

$$\mathrm{SFE}\ (\mathrm{yr}^{-1}) = \frac{\Sigma_{\mathrm{SFR}}}{\Sigma_{\mathrm{SMD}}}, \tag{7}$$

indicating the efficiency of gas consumption for the formation of stars. Rownd and Young (1999) have shown that SFE is roughly constant within galaxies, using 45″ resolution data. We show in figure 6 the change in SFE according to the distance from the center, using data in regions A through E. The radii for the plots are taken at the outer edge of each of the regions. Notice that the last panel in figure 6, with all of the

galaxies superposed, except those excluded in section 3, exhibit a roughly constant SFE of around 10^{-9} to 10^{-10} (yr^{-1}), even in the central regions, with an exception of several galaxies with an enhanced SFE. A constant SFE is a manifestation of the Schmidt law with an index $N = 1$, and shows that the gas-consumption timescale, τ, or the inverse of SFE, is about 1 to 10 Gyr through the entire disk and nucleus for most of the galaxies, and down to 0.1 Gyr for those galaxies with the enhanced SFE mentioned above.

5. Conclusions

We considered the relation between the gas content and the star-formation rate at high molecular densities in the central regions of 23 nearby normal spiral galaxies, using recent high-resolution CO observation data and combining it with previous single-dish observations. Our main results are as follows:

(1) The Schmidt law, or a simple power law of $\Sigma_{\rm SFR} \propto \Sigma_{\rm SMD}^{N}$, is found to be valid at densities of up to $\Sigma_{\rm SMD} \sim 10^{3} (M_{\odot}\,{\rm pc}^{-2})$ for normal spiral galaxies. Regardless of the radical physical differences to which these high density regions are subject, the Schmidt law index is found to be $N = 1.33 \pm 0.09$, with $N \sim 1$ in both the central and disk regions.

(2) IR luminous starbursts, which Kennicutt (1998) used to define a composite Schmidt law, is found to display a systematic difference compared to normal galaxies. These starbursts show systematically higher star-formation rates compared to that expected from the Schmidt law for normal spirals.

(3) The star-formation efficiency (SFE) was found to be roughly constant for more than half of our samples, consistent with the result by Rownd and Young (1999), even in the central few hundred parsecs of spirals. Several other galaxies show higher SFE in the central regions.

Further analysis of the Schmidt law, in order to gain insights into the physics of star formation depending on local physical states, should involve a galaxy sampled at multiple points within its disk, categorized by its characteristic physical conditions. A fundamental difficulty is that the Schmidt law has a time-averaged nature. The spatial resolution, velocity fields, and the local star-formation timescale can alter the relation between the gas and the star-formation tracers. If these uncertainties are removed, we may see sequential differences in the observed Schmidt law according to the physical conditions.

Although our results imply that starbursts display a different sequence of the gas–star formation rate relation compared to normal spirals, there are still uncertainties in the consistency between $\Sigma_{\rm SFR}$ derived from the IR and Hα luminosities, which are difficult to quantify. This is because the rate of gas clouds or dust covering a newly born OB star could alter the "true" star-formation rate when converted into IR or Hα luminosities. In order to compare normal and starburst galaxies in a more quantitative way, it will be important to use a uniform tracer of star formation.

The authors are grateful to T. Handa, for his enlightening comments on the Schmidt law index. H. Nakanishi and S. Onodera were financially supported by a Research Fellowship from the Japan Society for the Promotion of Science for Young Scientists.

References

Bloemen, J. B. G. M., et al. 1986, A&A, 154, 25
Bohlin, R. C., Savage, B. D., & Drake, J. F. 1978, ApJ, 224, 132
Boissier, S., Prantzos, N., Boselli, A., & Gavazzi, G. 2003, MNRAS, 346, 1215
Gao, Y., & Solomon, P. M. 2004, ApJ, 606, 271
Helfer, T. T., Thornley, M. D., Regan, M. W., Wong, T., Sheth, K., Vogel, S. N., Blitz, L., & Bock, D. C.-J. 2003, ApJS, 145, 259
Ho, L. C., Filippenko, A. V., & Sargent, W. L. W. 1997, ApJS, 112, 315
Kennicutt, R. C., Jr. 1989, ApJ, 344, 685
Kennicutt, R. C., Jr. 1998, ApJ, 498, 541
Kennicutt, R. C., Jr. & Kent, S. M. 1983, AJ, 88, 1094
Kent, S. M., Dame, T. M., & Fazio, G. 1991, ApJ, 378, 131
Kewley, L. J., Geller, M. J., Jansen, R. A., & Dopita, M. A. 2002, AJ, 124, 3135
Koopmann, R. A., Kenney, J. D. P., & Young, J. 2001, ApJS, 135, 125
Landolt, A. U. 1992, AJ, 104, 340
Nakai, N., & Kuno, N. 1995, PASJ, 47, 761
Nishiyama, K., & Nakai, N. 2001, PASJ, 53, 713
Rieke, G. H., & Lebofsky, M. J. 1985, ApJ, 288, 618
Rownd, B. K., & Young, J. S. 1999, AJ, 118, 670
Sakamoto, K., Okumura, S. K., Ishizuki, S., & Scoville, N. Z. 1999, ApJS, 124, 403
Sanders, D. B., Solomon, P. M., & Scoville, N. Z. 1984, ApJ, 276, 182
Schmidt, M. 1959, ApJ, 129, 243
Schultz, G. V., & Wiemer, W. 1975, A&A, 43, 133
Sneden, C., Gehrz, R. D., Hackwell, J. A., York, D. G., & Snow, T. P. 1978, ApJ, 223, 168
Solomon, P. M., Rivolo, A. R., Barrett, J., & Yahil, A. 1987, ApJ, 319, 730
Sofue, Y., Koda, J., Nakanishi, H., & Onodera, S. 2003b, PASJ, 55, 59
Sofue, Y., Koda, J., Nakanishi, H., Onodera, S., Kohno, K., Tomita, A., & Okumura, S. K. 2003a, PASJ, 55, 1189
Wong, T., & Blitz, L. 2002, ApJ, 569, 157
Young, J. S., et al. 1995, ApJS, 98, 219
Young, J. S., Allen, L., Kenney, J. D. P., Lesser, A., & Rownd, B. 1996, AJ, 112, 1903